Phase-Synchronization, Energy Cascade, and Intermittency in Solar-Wind Turbulence

S. Perri,[1] V. Carbone,[1,2] A. Vecchio,[1] R. Bruno,[3] H. Korth,[4] T. H. Zurbuchen,[5] and L. Sorriso-Valvo[2,6]

[1]*Dipartimento di Fisica, Università della Calabria, 87036 Rende (Cosenza), Italy*
[2]*IPCF-CNR, Ponte P. Bucci, Cubo 31C, 87036 Rende (Cosenza), Italy*
[3]*IFSI-INAF, Via Fosso del Cavaliere, I-00133 Roma, Italy*
[4]*The Johns Hopkins University Applied Physics Laboratory, Laurel, Maryland 20723, USA*
[5]*Department of Atmospheric, Oceanic, and Space Sciences, University of Michigan, Ann Arbor, Michigan 48109, USA*
[6]*Space Sciences Laboratory, University of California at Berkeley, 7 Gauss Way, Berkeley, 94720 California, USA*

(Received 31 May 2012; published 11 December 2012)

The energy cascade in solar wind magnetic turbulence is investigated using MESSENGER data in the inner heliosphere. The decomposition of magnetic field time series in intrinsic functions, each characterized by a typical time scale, reveals phase reorganization. This allows for the identification of structures of all sizes generated by the nonlinear turbulent cascade, covering both the inertial and the dispersive ranges of the turbulent magnetic power spectrum. We find that the correlation (or anticorrelation) of phases occurs between pairs of neighboring time scales, whenever localized peaks of magnetic energy are present at both scales, consistent with the local character of the energy transfer process.

DOI: 10.1103/PhysRevLett.109.245004 PACS numbers: 94.05.Lk, 52.35.Ra

The mechanism of turbulent energy cascade in fluids [1] and in magnetized fluid flows [2] is still poorly understood. This process involves many coupled degrees of freedom and exhibits universal and nontrivial scaling behavior [1,3]. According to Richardson's phenomenology [4], the turbulent energy cascades from eddies at a scale ℓ to eddies at smaller (but comparable) scales $\ell' < \ell$ [5]. Experiments suggest that the energy transfer is not steady but intermittent, exhibiting strong bursts of activity in between relatively quiescent periods [1,6]. The nonhomogeneity of the energy transfer is described, for example, by the multifractal model [7], which takes into account the concentration of energy in ''active eddies'' [1] while cascading towards smaller scales. According to the multifractal model, the energy cascade spontaneously generates isolated bursts of fluctuations on all spatial scales [8,9].

In order to identify turbulent structures in experimental data, intermittent bursts of turbulent activity have often been related to the presence of convected coherent structures such as ribbons, tubes, or sheets of vorticity, as well as localized current sheets in magnetized fluids [2,9,10]. Such structures of a given scale are generally considered as isolated features embedded in a random Gaussian background [11]. Arbitrary threshold methods are commonly used to detect isolated structures, which should be characterized by phase correlations in the field [2]. In the solar wind, those isolated structures can develop in the process of the turbulent energy cascade down to smaller scales, although the existence of structures of solar origin, generated at relatively large scale and not arising from a cascade process, cannot be ruled out. On the other hand, the presence of the energy cascade is associated with the scaling of the third-order structure function (Yaglom's law) [1,12], which has no intermittent corrections. Yaglom's law suggests that fluctuations are generated *on all scales* by the cascade process and that fluctuations on different scales should be somehow connected, for example, through phase synchronization.

The solar wind represents the largest laboratory for direct investigation of plasma turbulence [2]. The degree of complexity is enhanced by the existence of many characteristic scales, related to different physical processes. This means that the mechanism of energy transfer among scales depends on the scale itself. Indeed, within the Please note that, as the acronym magnetohydrodynamic has been used less than three times in this letter, it has been deleted and replaced with its definition. Please check and verify that no meaning has been altered.magnetohydrodynamic range, solar wind turbulence exhibits a Kolmogorov-like power law energy spectrum in the wave vector k space, $\sim k^{-5/3}$ [2], while, in the dissipative (or dispersive) range, the spectrum steepens beyond the proton scales ($\sim k^{-\alpha}$, with $\alpha \in [2, 4]$) [13,14]. In this Letter, we show the first evidence of phase synchronization between structures on different scales in solar wind, generated by the turbulent cascade of magnetic energy.

Our analysis of solar wind data is based on the combined use of the empirical mode decomposition (EMD) [15] and of wavelet analysis [16]. The former provides a decomposition of solar wind turbulent fields in a limited number of modes (including information on the phase), while the latter enables the detection of intermittent structures and energy transfer in the flow. EMD was originally developed to process nonstationary and nonlinear data [15], such as experimental turbulence records [17]. However, it has been further applied successfully to a variety of physical systems [18–21]. A turbulent field $B(t)$ is decomposed into a finite number n of intrinsic mode functions (IMFs), as

$$B(t) = \sum_{j=1}^{n} \mathrm{IMF}_j(t) + r_n(t). \quad (1)$$

IMFs can be written as $\mathrm{IMF}_j(t) = A_j(t)\cos\Phi_j(t)$, where $A_j(t)$ and $\Phi_j(t)$ represent the amplitude and the phase of the jth mode, respectively; thus, they are zero-mean oscillating functions, experiencing both amplitude and frequency modulations. Each IMF is characterized by a time-dependent $\omega_j(t)$, and a typical time scale can be obtained by averaging over the whole time interval. Therefore, at variance with the classical Fourier decomposition, the characteristic time scale τ_j for IMFs is an average time scale. The residue $r_n(t)$ in Eq. (1) describes the mean trend. EMD is local, complete, and orthogonal. It therefore allows the reconstruction of the signal through partial sums in Eq. (1). When applied to real data, the dynamic behavior of the system is represented by a limited number of modes n.

Wavelet analysis, on the other hand, provides useful information on the frequency and time energy distribution of a time series. In order to identify intermittent bursts of energy at different time scales, the local intermittency measure (LIM) [16,22] has been applied to turbulent data. The LIM is defined as

$$\mathrm{LIM}_{\tau,t} = \frac{|\tilde{b}_{\tau,t}|^2}{\langle|\tilde{b}_{\tau,t}|^2\rangle_t}, \quad (2)$$

where $\tilde{b}_{\tau,t}$ is the wavelet coefficient of a component of the magnetic field vector at time t and time scale τ. The angled brackets in Eq. (2) indicate the time average. For each frequency $1/\tau$, the condition $\mathrm{LIM} > 1$ identifies portions of the sample whose power (estimated as the squared wavelet coefficient) is above the average, within the time series. Therefore, such portions may represent intermittent structures, where magnetic energy accumulates [23] during the nonlinear energy cascade.

In this Letter, we proceed as follows: after applying EMD to each solar wind magnetic field vector component, we investigate the phase difference of IMFs at two neighboring time scales (τ_i, τ_j). Then, we look for the simultaneous presence of intermittent structures at the same pair of neighboring time scales, as detected by LIM, being an indication of energy transfer between such scales.

For our study, we analyze solar wind magnetic field measurements in the inner heliosphere, using 2 Hz sampled data from the magnetometer onboard the MESSENGER spacecraft [24]. The sample was taken at a heliocentric distance of about 0.3 A.U., far away from the planet Mercury. The magnetic field components in the radial-tangential-normal reference frame are shown in the left panel of Fig. 1. In this frame, R indicates the radial antisunward direction, T is the tangential direction obtained from the cross product between the solar rotation axis and R, and N completes the frame. The time interval refers to an observation made on January 14th, 2010, from 00:00:00 to 01:06:00 UT, near the minimum of solar cycle 23. The magnetic field magnitude (black solid line) is rather steady, while the tangential (blue dotted line) and normal (green dashed-dotted line) components fluctuate around zero. Notice that the large scale mean magnetic field (the Parker spiral) is roughly radial near 0.3 A.U. Therefore, the magnetic field variance is larger in the plane perpendicular to the mean field, indicating the presence of Alfvénic fluctuations [2]. The right panel of Fig. 1 shows the power spectral density (PSD) of the tangential component of **B**. The best power law fits are also indicated, both in the inertial range (thick solid red line) and in the high frequency range (thick dashed blue line), with a break at $f_{\mathrm{br}} \sim 0.2$ Hz [25,26]. It is important to remark that the spectrum

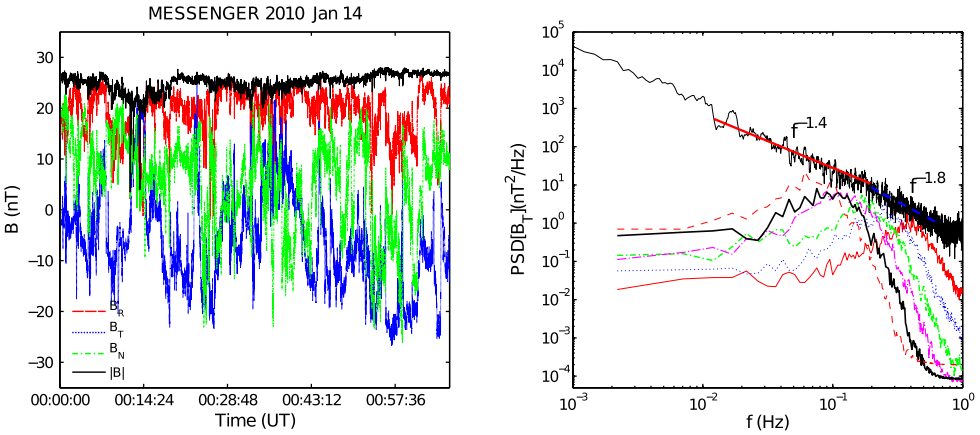

FIG. 1 (color online). Time evolution of the magnetic field components in the radial-tangential-normal reference frame and of the magnetic field magnitude (left panel). The power spectrum of the B_T component along with the power law best fits both in the inertial (thick solid red line) and in the high frequency range (thick dashed blue line) (right panel). In the right panel, the spectra of IMFs above and below the spectral break frequency are also displayed (thin solid red, dotted blue, dashed-dotted green, long-dashed-dotted magenta, thick solid black, and dashed red lines). For example, the thin solid red curve has a peak around 0.4 Hz, which is the average frequency of the highest frequency mode computed.

corresponds in frequency to the spectrum in the k vector space, assuming that the Taylor hypothesis applies [27]. High amplitude magnetic field fluctuations, described by a Kolmogorov-like energy spectrum, confirm that the sample is turbulent.

The EMD of the tangential magnetic field component B_T gives $n = 18$ significant modes. In order to estimate the typical time scales, for each IMF the PSD [15] was computed (see the right panel of Fig. 1). The modes display power either in the high frequency range (from ~0.2 to 0.45 Hz) or in the inertial range (from 0.01 to 0.1 Hz). The position in frequency, f_i, of the peak of the PSDs of the modes (see the thin solid red, dotted blue, dashed-dotted green, long-dashed-dotted magenta, thick solid black, and dashed red lines in the right panel of Fig. 1) gives an estimate of the characteristic time scale of each mode, $\tau_i = 1/f_i$. Therefore, IMFs with f_i above the spectral break of B_T "track" the small scale fluctuations of the field [15]. Going to lower frequencies, the large scale fluctuations of the B_T time series show up in the IMFs (not shown). Three pairs of phases of IMFs (Φ_i, Φ_j) associated with neighboring time scales are plotted in Fig. 2, along with the absolute value of their phase difference $\Delta\phi \equiv \Phi_i - \Phi_j$. The left panels of Fig. 2 refer to a pair of next-nearest time scales in the high frequency range of the magnetic field spectrum, the middle panels to a pair of adjacent time scales within the inertial range, and the right panels to one scale τ_i in the inertial range and another scale τ_j in the high frequency range. Application of the LIM to B_T provides the location of the peaks of power in the time series. We then locate the occurrence of simultaneous LIM peaks in the chosen pairs of time scales (τ_i, τ_j), as shown in top panels of Fig. 2, indicating an energy transfer between the two scales.

In the left and middle columns of Fig. 2, simultaneous LIM peaks (top row) are found when the two mode phases overlap (middle row), the phase difference becoming negligible (bottom row). This has been highlighted in Fig. 2 through green frames. Thus, in the locations where energy is being transferred between two scales, as evidenced through simultaneous LIM peaks, phase synchronization between the modes of the field fluctuations occurs. On the contrary, phase synchronization is not correlated to LIM peaks for pairs of well separated time scales (right column of Fig. 2), in agreement with a local nonlinear energy cascade. It is important to point out that phase synchronization is observed regardless of the LIM peak amplitude (see the upper left panel of Fig. 2). In the framework of the multifractal energy cascade, this suggests that small intensity structures, showing phase synchronization, are also generated in the flow. Similar results hold for B_R and B_N components (not shown).

To quantitatively confirm the observation of phase synchronization, we look for statistical correlations between the phase difference of each pair of modes (IMF_i, IMF_j) and the LIM covariance at the same time scales, defined as

$$\mathrm{Covar}\,(\mathrm{LIM}_i, \mathrm{LIM}_j) = \mathrm{LIM}_i(t) \times \mathrm{LIM}_j(t). \qquad (3)$$

In Fig. 3, we plot, for the three examples given above, the rate of occurrence of binned pairs [$|\Delta\phi|$, $\mathrm{Covar}(\mathrm{LIM}_i, \mathrm{LIM}_j)$]. For the two cases with next-nearest modes, (IMF_2, IMF_3) and (IMF_8, IMF_9) in the high frequency and in the inertial ranges, respectively, the majority of pairs have phase synchronization (small $|\Delta\phi|$), with a secondary peak at $\sim\pi$, indicating phase anticorrelation. On the contrary, the histogram for the pair (IMF_2, IMF_5), referring to separated time scales, is broad in $|\Delta\phi|$, indicating an absence of correlation between phase difference and LIM coupled peaks.

The analysis of solar wind magnetic turbulence in the inner heliosphere through coupled EMD and wavelet analyses evidences that modes of the signal on neighboring time scales have phase synchronization whenever localized

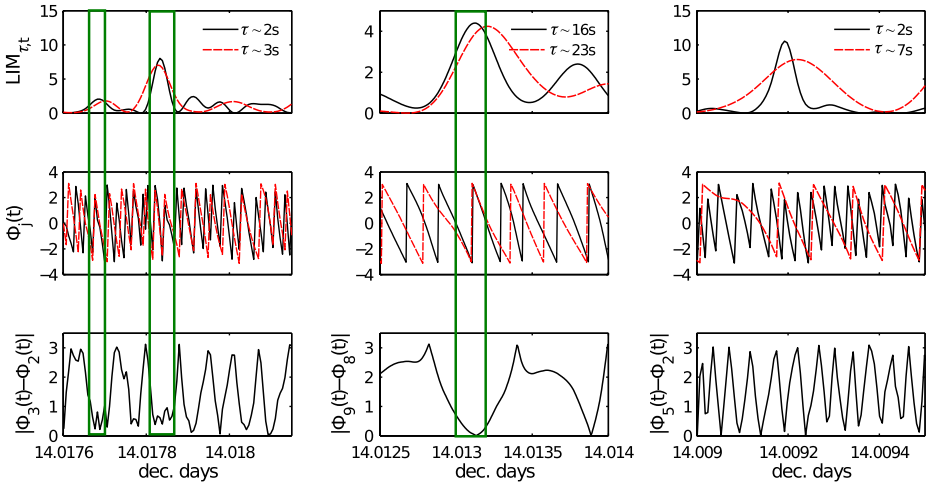

FIG. 2 (color online). Top panels: LIM as a function of time t at two different time scales τ (see the legend). Middle panels: phases Φ_j of the IMFs at the τ indicated in the top panels. Bottom panels: absolute value of the phase difference of the two IMFs. Notation: the subscript j indicates the number of the mode; for example, $\Phi_9(t)$ is the mode number 9 having a typical time scale $\tau \sim 23$ s.

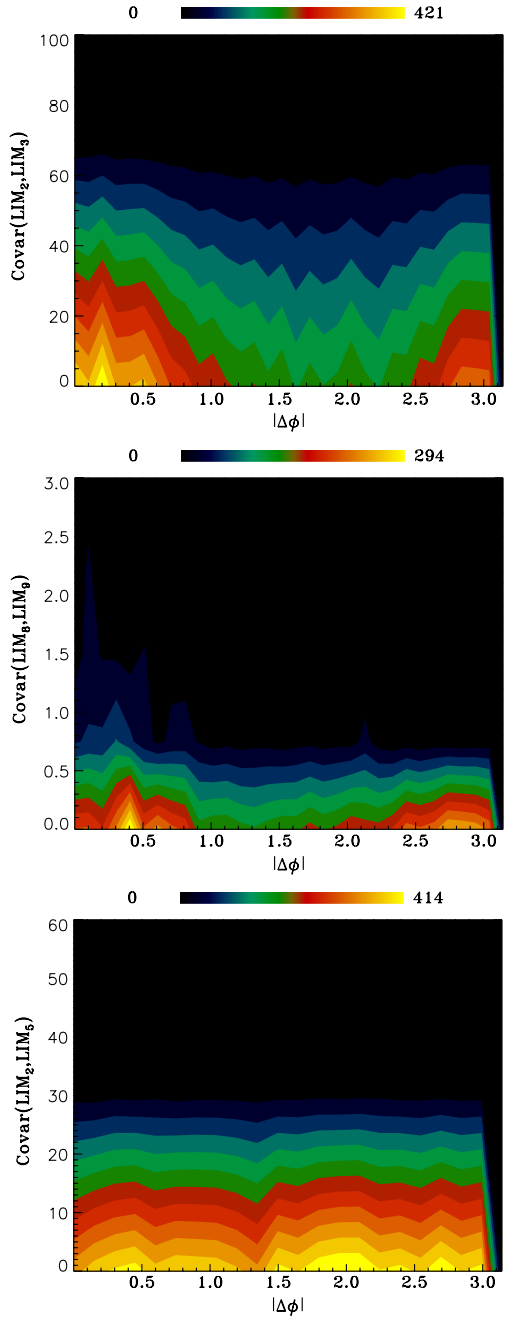

FIG. 3 (color online). 2D histograms $[|\Delta\phi|, \mathrm{Covar}(\mathrm{LIM}_i, \mathrm{LIM}_j)]$ for the three cases displayed in Figure 2. The intensity of the colorbar (from dark to bright) refers to the number of events stored in each bidimensional bin.

peaks of magnetic energy transfer occur, regardless of their amplitude. This allows the identification of magnetic eddies generated by the turbulent cascade at different scales and characterized by phase synchronization.

In order to test our results, the same EMD and LIM analyses have also been applied to two synthetic data sets. The first data set is a Gaussian, self-similar Wiener process [28], with no intermittent structures. The second set is an intermittent field generated through simple superposition of a Gaussian background and coherent structures sharing the same statistical properties of solar wind magnetic fluctuations (see Ref. [29] for details). In this sample, intermittency is not the result of a cascade but is simply built to mimic the statistical features of an intermittent field. Phase synchronization is not observed to be correlated to the LIM peaks in either of the data sets (see Ref. [30] the Supplemental Material, Figs. 1s and 2s for the Gaussian background + coherent structure model and Fig. 3s for the Wiener process). This confirms that phase synchronization observed in solar wind data is entirely due to the nonlinear energy turbulent cascade, which is not present in the synthetic data.

The detection and analysis of large amplitude structures in turbulent flows are usually based upon arbitrary intensity threshold techniques [9,22,31], which are able to eliminate intermittency and multifractality from the time series. These methods capture the extreme events, contained in the tails of the probability distribution functions of fluctuations, which dominate higher-order statistics. Our analysis shows that phase synchronization is observed during the occurrence of bursts of magnetic energy of any amplitude, i.e., for the whole probability distribution function, giving information on the nonlinear energy transfer through the scales.

The results shown here indicate the presence of significant phase synchronization only for comparable time scales. This is consistent with the classical picture of the local turbulent energy cascade, where nonlinear interactions mostly occur between next-nearest wave vectors [1].

Finally, phase correlation between adjacent modes is found both in the magnetohydrodynamic inertial range and in the high frequency range of solar wind magnetic turbulence. This confirms that a nonlinear turbulent cascade is active well beyond the high frequency break (i.e., at proton scales) of the solar wind magnetic field power spectrum [14,32], whose nature is still a matter of debate.

This work was partially supported by the Italian Space Agency, ASI Contract No. I/015/07/0 "Esplorazione del Sistema Solare." The research of S. P. and A. V. is supported by "Borsa Post-doc POR Calabria FSE 2007/2013 Asse IV Capitale Umano - Obiettivo Operativo M.2." S. P., V. C., R. B., and L. S. V. acknowledge their participation in the ISSI team 185. S. P., V. C., and L. S. V. acknowledge the Marie Curie Project FP7 PIRSES-2010-269297. The authors further acknowledge the NASA Planetary Data System for the use of the MESSENGER data.

[1] U. Frisch, *Turbulence: The Legacy*, edited by A. N. Kolmogorov (Cambridge University Press, Cambridge, England, 1995).
[2] R. Bruno and V. Carbone, Living Rev. Solar Phys. **2**, 1 (2005).
[3] A.-N. Kolmogorov, Dokl. Akad. Nauk SSSR **30**, 301 (1941).

[4] L.-F. Richardson, *Weather Prediction by Numerical Process* (Cambridge University Press, Cambridge, England, 1922).
[5] E.-A. Novikov, Sov. Phys. Dokl. **14**, 104 (1969).
[6] G.-K. Batchelor and A.-A. Townsend, Proc. R. Soc. A **199**, 238 (1949).
[7] G. Parisi and U. Frisch, in *Proceedings of the International School of Physics "Enrico Fermi"* edited by M. Ghil, R. Benzi, and G. Parisi (North-Holland, Amsterdam, 1983).
[8] V. Carbone, P. Veltri, and R. Bruno, Phys. Rev. Lett. **75**, 3110 (1995).
[9] P. Veltri and A. Mangeney, in *Solar Wind Nine*, AIP Conf. Proc. Vol. 471, edited by S.-R. Habbal, J.-V. Hollweg, and P.-A. Isenberg (AIP, New York, 1999).
[10] A. Y.-S. Kuo and S. Corrsin, J. Fluid Mech. **50**, 285 (1971).
[11] R. Bruno, V. Carbone, P. Veltri, E. Pietropaolo, and B. Bavassano, Planet. Space Sci. **49**, 1201 (2001).
[12] L. Sorriso-Valvo, R. Marino, V. Carbone, A. Noullez, F. Lepreti, P. Veltri, R. Bruno, B. Bavassano, and E. Pietropaolo, Phys. Rev. Lett. **99**, 115001 (2007).
[13] R.-J. Leamon, C. W. Smith, N. F. Ness, W. H. Matthaeus, and H. K. Wong, J. Geophys. Res. **103**, 4775 (1998).
[14] O. Alexandrova, V. Carbone, P. Veltri, and L. Sorriso-Valvo, Astrophys. J. **674**, 1153 (2008).
[15] N.-E. Huang, Z. Shen, S. R. Long, M. C. Wu, H. H. Shih, Q. Zheng, N.-C. Yen, C. C. Tung, and H. H. Liu, Proc. R. Soc. A **454**, 903 (1998).
[16] M. Farge, M. Holschneider, and J.-F. Colonna, in *Topological Fluid Mechanics*, edited by H.-K. Moffat (Cambridge University Press, Cambridge, England, 1990).
[17] F. Foucher and P. Ravier, Exp. Fluids **49**, 379 (2010).
[18] D.-A.-T. Cummings, R. A. Irizarry, N. E. Huang, T. P. Endy, A. Nisalak, K. Ungchusak, and D. S. Burke, Nature (London) **427**, 344 (2004).
[19] A. Vecchio, M. Laurenza, V. Carbone, and M. Storini, Astrophys. J. Lett. **709**, L1 (2010).
[20] M. Onofri, A. Vecchio, G. D. Masi, and P. Veltri, Astrophys. J. **746**, 58 (2012).
[21] A. Vecchio, M. Laurenza, D. Meduri, V. Carbone, and M. Storini, Astrophys. J. **749**, 27 (2012).
[22] M. Onorato, R. Camussi, and G. Iuso, Phys. Rev. E **61**, 1447 (2000).
[23] R. Bruno *et al.*, *Proceedings of the 9th European Meeting on Solar Physics, Florence, Italy, 1999*, edited by A. Wilson, (European Space Agency, Noordwijk, 1999).
[24] B. J. Anderson, M. H. Acuña, D. A. Lohr, J. Scheifele, A. Raval, H. Korth, and J. A. Slavin, Space Sci. Rev. **131**, 417 (2007).
[25] S. Perri, V. Carbone, and P. Veltri, Astrophys. J. Lett. **725**, L52 (2010).
[26] H. Korth, B. J. Anderson, T. H. Zurbuchen, J. A. Slavin, S. Perri, S. A. Boardsen, D. N. Baker, S. C. Solomon, and R. L. McNutt, Planet. Space Sci. **59**, 2075 (2011).
[27] G.-I. Taylor, Proc. R. Soc. A **164**, 476 (1938).
[28] C.-W. Gardiner, *Handbook of Stochastic Methods* (Springer, New York, 1997).
[29] R. Bruno, V. Carbone, L. Primavera, F. Malara, L. Sorriso-Valvo, B. Bavassano, and P. Veltri, Ann. Geophys. **22**, 3751 (2004).
[30] See Supplemental Material at http://link.aps.org/supplemental/10.1103/PhysRevLett.109.245004 for the results of the analysis performed on a synthetic time series consisting of a superposition of a Gaussian background and coherent structures (Fig. 1s shows that peaks in the LIM are not associated with phase synchronization in the IMFs; Fig. 2 reports that no correlation between the LIM covariance and the absolute value of the phase difference of neighboring modes is observed), and on a synthetic monofractal Wiener process (Fig. 3s shows again that no correlation between the LIM covariance and the phase differences exists).
[31] C. Salem, A. Mangeney, S.-D. Bale, and P. Veltri, Astrophys. J. **702**, 537 (2009).
[32] F. Sahraoui, M. L. Goldstein, P. Robert, and Y. V. Khotyaintsev, Phys. Rev. Lett. **102**, 231102 (2009).